ISBN: 978-3-95450-241-7 ISSN: 2673-5350 doi:10.18429/JACoW-IBIC2022-WE1C2

AN X-RAY BEAM PROPERTY ANALYZER BASED ON DISPERSIVE CRYSTAL DIFFRACTION

N. Samadi†, C. Ozkan Loch, G. Lovric, Paul Scherrer Institut (PSI), Villigen PSI, Switzerland
X. Shi, Advanced Photon Source, Argonne National Laboratory, Lemont, USA

Abstract

The advance in low-emittance X-ray sources urges the development of novel diagnostic techniques. Existing systems either have limited resolution or rely heavily on the quality of the optical system. An X-ray beam property analyzer based on a multi-crystal diffraction geometry was recently introduced. By measuring the transmitted beam profile of a dispersive Laue crystal downstream of a double-crystal monochromator, the system can provide a high-sensitivity characterization of spatial source properties, namely, size, divergence, position, and angle in the diffraction plane of the system at a single location in a beamline. In this work, we present the experimental validation at a super-bending magnet beamline at the Swiss Light Source and refine the method to allow for time-resolved characterization of the beam. Simulations are then carried out to show that the system is feasible to characterize source properties at undulator beamlines for fourth-generation light sources.

INTRODUCTION

Fourth-generation synchrotron facilities [1-3] have brought the needs and challenges in developing advanced source property diagnostics. A complete characterization of the source position, angle, size, and divergence is critical for not only the electron source study but also the beamline experiment optimization. Many efforts have been dedicated to searching for the best diagnostic tools with different approaches, such as direct imaging [4-6], interferometry-based [7-9], and dispersion-based methods [10, 11]. Since each technique has advantages and limitations, we have concluded in a recent review [12] that the combination of multiple techniques may be advantageous.

Most recently, an X-ray beam property analyzer (XBPA) based on a multi-crystal diffraction geometry has been proposed and demonstrated to measure source properties with high resolution and sensitivity [13], showing great potential for X-ray beam quality characterization at next-generation light sources. Here, we first review the theoretical model of the XBPA system, followed by an experimental demonstration at a super-bending magnet beamline at the Swiss Light Source (SLS), performed with an ultra-fast detector. Finally, we summarize the simulation results of the XBPA for analyzing the source properties of an undulator beamline, as proposed in the course of the SLS upgrade.

XBPA SYSTEM DESCRIPTION

The XBPA system together with the physical model and fundamental equations is described in detail in [13]. A schematic is shown in Fig. 1. The XBPA system uses a crystal monochromator (e.g., a double-crystal monochromator (DCM) is the most commonly used) to generate a narrow-bandwidth (in the order of $\Delta E/E \approx 10^{-4}$) beam with the energy spread in the diffraction direction (e.g., vertical direction for a vertical deflecting monochromator), as shown in Fig. 1(a). The flat beam downstream of the monochromator is a near-Gaussian profile, as shown in Fig. 1(b), that contains the source angle and divergence information. By placing a Laue crystal in the dispersion geometry tuned to the central energy of the monochromator, a small spatial portion of the beam will be diffracted away, leaving a valley in the transmitted beam profile, as shown in Fig. 1(c). The width and location of the valley contain the source position and size information. By analyzing both the flat and transmitted beam profiles, the spatial properties of the photon source in the diffraction direction can be fully extracted.

When the source has a fixed position, but the beam is tilted by an angle, the flat beam will move vertically according to the angle and the source-to-detector distance. However, the Laue-transmitted beam valley location will not move, as the monochromator will select out the same energy from the angular distribution of the source, or the central energy line (dashed line in Fig. 1) will not move. On the other hand, if the source is fixed in angle but moves vertically in position, not only the flat beam will move vertically, but the valley position will also move vertically the same amount as the source motion (i.e., a parallel vertical shift of the dashed central energy line in Fig. 1). Thus, there is a simple relationship between the vertical source angle (y_s') and position (y_s) and the measured flat beam location

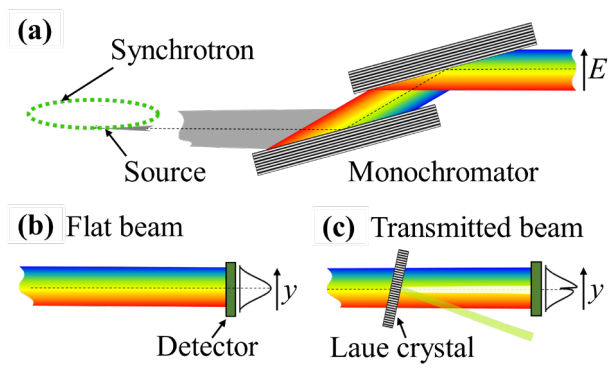

Figure 1: Schematic of the XBPA system containing the crystal monochromator, the Laue crystal in dispersion geometry downstream of the monochromator, and the detector. (a) shows a double-crystal monochromator geometry, (b) and (c) show the flat beam without the Laue crystal and the transmitted beam with the Laue crystal tuned to the central energy of the monochromator, respectively.

† nazanin.samadi@psi.ch

Content from this work may be used under the terms of the CC BY 4.0 licence (© 2022). Any distribution of this work must maintain attribution to the author(s), title of the work, publisher, and DOI

ISBN: 978-3-95450-241-7 ISSN: 2673-5350 doi:10.18429/JACoW-IBIC2022-WE1C2

(y_{flat}) and Laue-transmitted beam vally location (y_{valley}). This can then be used to determine the vertical source position and angle [13] by,

$$y_s = y_{\mathrm{valley}} \tag{1}$$

and

$$y_s' = \frac{y_{\mathrm{flat}} - y_s}{d}, \tag{2}$$

where d is the source-to-detector distance.

Similarly, the source size and divergence information can be extracted from the measured flat beam profile and the Laue-transmitted beam (valley) profile. Since the valley profile is not Gaussian, a simple Gaussian fitting will not work. Instead, we extract the source profile $I_s(y)$ through curve fitting the measured valley profile $I_{\mathrm{valley}}(y)$ given by,

$$I_{\mathrm{valley}}(y) = \frac{I_{\mathrm{trans}}(y)}{I_{\mathrm{flat}}(y)}, \tag{3}$$

where $I_{\mathrm{trans}}(y)$ and $I_{\mathrm{flat}}(y)$ are the measured Laue-transmitted and flat beam profiles, respectively. The curve fitting is performed by minimizing the error function in a discrete form defined as [13],

$$err = \left\{\frac{1}{n}\sum_{i=1}^{n}\left[I_{\mathrm{point}}(y_i) * I_s(y_i) - I_{\mathrm{valley}}(y_i)\right]^2\right\}^{1/2}, \tag{4}$$

where i is the pixel index on the detector along the vertical direction, n is the total number of pixels and $*$ is the convolution operator. The $I_{\mathrm{point}}(y)$ is the theoretical valley profile that can be accurately calculated using dynamical theory [14]. Assuming a Gaussian source profile,

$$I_s(y) = \exp\left[-\frac{(y - y_s)^2}{2\sigma_y^2}\right]. \tag{5}$$

The sigma source size σ_y can thus be extracted from the curve fitting process. Finally, the source divergence $\sigma_{y'}$ can be derived from the flat beam size, σ_{flat}, assuming a Gaussian flat beam distribution, given by,

$$\sigma_{y'} = \frac{1}{d}\left(\sigma_{\mathrm{flat}}^2 - \sigma_y^2\right)^{1/2}.$$

EXPERIMENTAL DEMONSTRATION

The first experimental demonstration of the XBPA system was carried out at the SLS optics beamline (X05DA dipole magnet) [15], and the results were reported in [13]. Here we show data from a new experiment performed at the X02DA TOMCAT beamline (2.9 Tesla super-bending magnet) at the SLS. A Si (1,1,1) fixed-exit double-crystal monochromator (DCM) at approximately 7 m from the source was used to tune the X-ray energy to around 20 keV. A 1× objective lens coupled to a 300-micron LuAG scintillator and an ultra-fast CMOS detector [16] was used to capture images with an effective pixel size of 11×11 μm^2.

A 350 μm thick Si (1,1,1) Laue crystal was placed in a dispersive geometry against the DCM at 25.1 m from the source. The Laue crystal was tuned to the central energy of the DCM to diffract at 20 keV. The detector was placed at 25.2 m from the source and collected the flat beam (without the Laue crystal) and the transmitted beam images through the Laue crystal. The measurements were performed with different acquisition times (down to milliseconds level), thanks to the high flux provided by the super-bending magnet source. The results presented here use an acquisition time of 40 ms for a single image.

Figure 2(a) shows the dark-corrected flat beam image and its integrated 1D profile, $I_{\mathrm{flat}}(y)$, (black dashed curve), and Figure 2(b) shows the dark-corrected transmitted beam image through the Laue crystal with its integrated 1D profile, $I_{\mathrm{trans}}(y)$, (black solid curve). Note that the 1D profiles were obtained by integrating over the central 500 horizontal pixels of each 2D beam image. Figure 2(c) shows the valley profile, $I_{\mathrm{valley}}(y)$, (solid curve) and the numerically fitted profile (dashed curve). The vertical source size was measured to be σ_y = 17±2 μm (rms), as compared to a recent result (17-18 μm rms) using zone plate imaging [17] and the previously measured values (15 μm rms, or 35 μm FWHM) based on the fractional Talbot effect [18]. The error bar was determined as the standard deviation of 20 measurements (each measurement was an average of 10 images). Note that the beam profile in Fig. 2(a) is not a perfect Gaussian shape with a brighter central part, which is caused by the superposition of the third-harmonic beam (Si(3,3,3) diffraction of the 60 keV beam). Thus, the fitting has been performed using Eq. (4) with $I_{\mathrm{point}}(y)$ constructed as a sum of the first and the third harmonic contributions assuming a specific ratio (4:1, estimated from the bending magnet spectrum and scintillator photon yield).

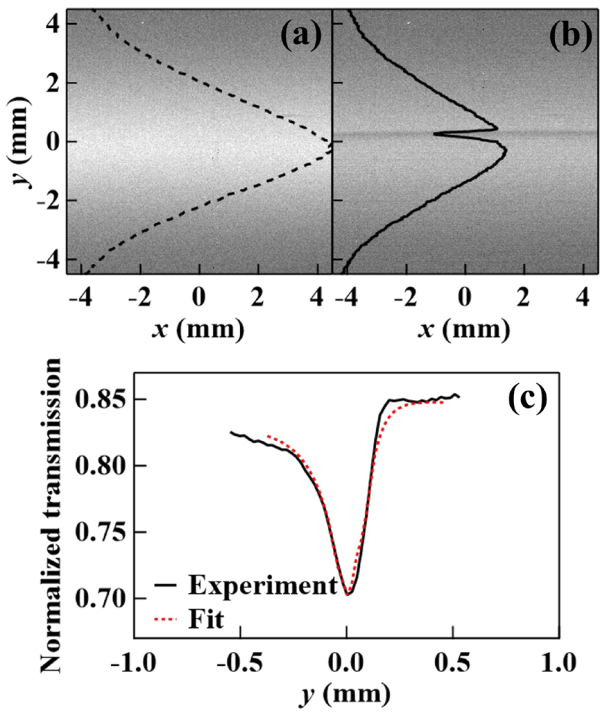

Figure 2: Images of (a) the flat beam and its 1D integrated profile, $I_{\mathrm{flat}}(y)$, (dashed curve) and (b) the Laue-transmitted beam and its 1D integrated profile, $I_{\mathrm{trans}}(y)$, (solid curve). (c) Normalized transmission (valley) profiles from the experiment, $I_{\mathrm{valley}}(y)$, (solid curve) the numerical fit (dashed curve).

Content from this work may be used under the terms of the CC BY 4.0 licence (© 2022). Any distribution of this work must maintain attribution to the author(s), title of the work, publisher, and DOI

ISBN: 978-3-95450-241-7 ISSN: 2673-5350 doi:10.18429/JACoW-IBIC2022-WE1C2

Content from this work may be used under the terms of the CC BY 4.0 licence (© 2022). Any distribution of this work must maintain attribution to the author(s), title of the work, publisher, and DOI

Since the bending magnet source size is dominated by the electron beam, $I_s(y)$ in Eq (4) stays the same.

UNDULATOR SOURCE PROPERTY CHARACTERIZATION

The resolution of the XBPA system is determined by the diffraction bandwidth of the monochromator and Laue crystal. In order to measure an undulator source, especially at low-emittance light sources, the crystal bandwidth has to be significantly smaller than the angular divergence of the source. Otherwise, the valley in the transmitted beam may be too wide compared to the beam width, which makes it challenging to extract the valley profile using Eq. (3). One solution is to use a high-index reflection of the crystals.

We next simulate the feasibility of the XBPA system in measuring undulator source properties using the *Shadow-Oui* ray-tracing program [19] in the *OASYS* environment [20]. The photon source parameters (including both contributions from the electron and undulator radiation) used are σ_y= 5.9 µm and $\sigma_{y'}$ = 3.6 µrad. The monochromator is a Si(333) Bragg DCM, and the Laue crystal is a symmetric Si(333) Laue crystal with a thickness of 0.25 mm. The diffraction/transmission profiles of the Laue crystal are generated by the *XCRYSTAL* module [21] before being used in the ray tracing. The detector is at d = 15 m from the source. For each simulation, 5×10^6 rays are used to achieve sufficient statistics.

Five sets of simulations (virtual experiments) were carried out: (1) the nominal case with no source parameter changes, (2) the source position y_s shifted by 1.77 µm, (3) the source angle y_s' tilted by 0.57 µrad, (4) the source size reduced to σ_y= 4.72 µm, and (5) the source divergence reduced to $\sigma_{y'}$= 3.43 µrad. The simulated flat beam profiles and transmission profiles are shown in Fig. 3. The extracted source parameters are summarized in Table 1. The XBPA system can correctly isolate and measure source position, angle, size, and divergence changes, making it a promising source diagnostic tool for undulator sources.

Table 1: Results of Source Property Simulation

#	Input change	Output (extracted from simulation)
(1)	σ_y = 5.9 µm $\sigma_{y'}$ = 3.6 µrad	y_s = 0, y_s' = 0 σ_y = 5.72 µm, $\sigma_{y'}$ = 3.64 µrad
(2)	y_s = 1.77 µm	y_s = 1.76 µm, $\Delta y_s'$ = −0.003 µrad
(3)	y_s' = 0.57 µrad	Δy_s = 0.00 µm, y_s' = 0.565 µrad
(4)	σ_y = 4.72 µm	σ_y = 4.66 µm, $\Delta\sigma_{y'}$ = 0.004 µrad
(5)	$\sigma_{y'}$ = 3.43 µrad	$\Delta\sigma_y$ = 0.11 µm, $\sigma_{y'}$ = 3.47 µrad

CONCLUSION

Here we have described how the XBPA system can be used to characterize the source properties at synchrotron light sources. Measurements of the TOMCAT super bending magnet beamline source size have been demonstrated and give a good agreement with previous results. Simulations were conducted to show the feasibility of using the XBPA system to characterize the undulator source position, angle, size, and divergence at low-emittance light sources. The XBPA system is a promising source diagnostic tool for different beamlines and photon energies.

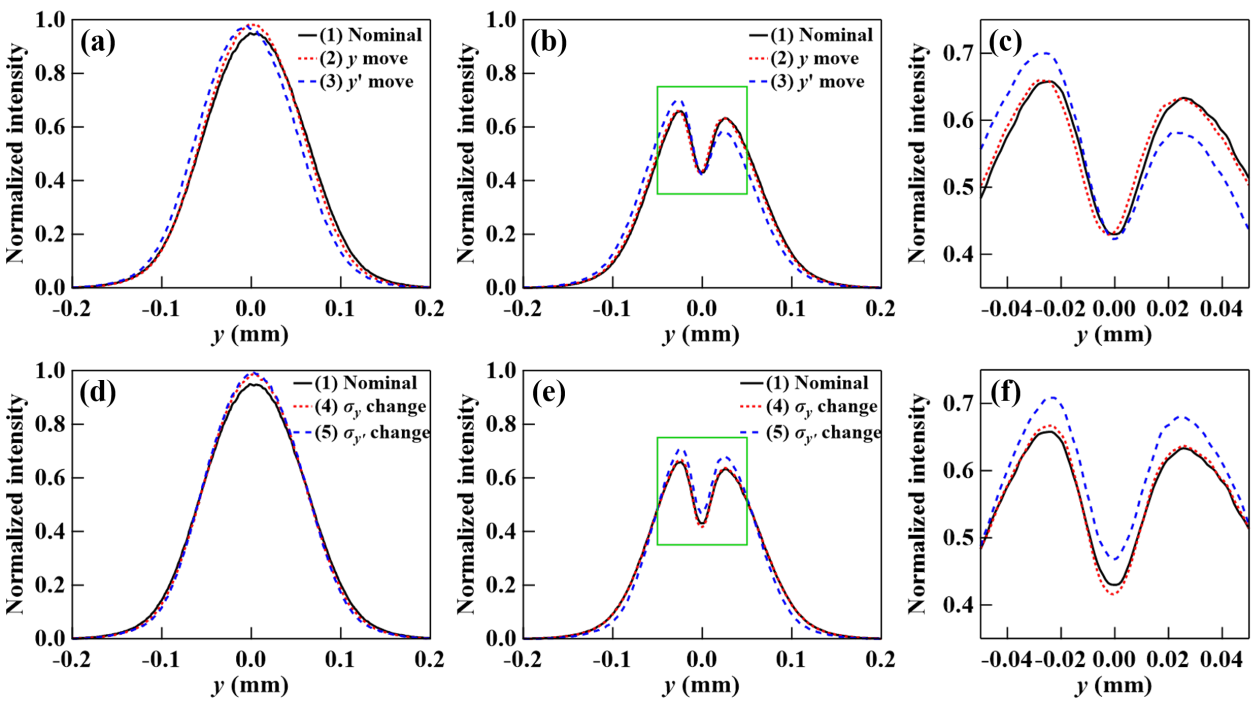

Figure 3: Simulated flat beam profiles (a and d) and Laue-transmitted beam profiles (b and e) of an undulator with different source parameters (see text and Table 1 for details of the five sets of simulations). Figures (c) and (f) are the enlarged regions (green boxes) of (b) and (e), respectively.

ISBN: 978-3-95450-241-7 ISSN: 2673-5350 doi:10.18429/JACoW-IBIC2022-WE1C2

REFERENCES

[1] M. Eriksson, J. F. Van Der Veen, and C. Quitmann, *"Diffraction-Limited Storage Rings-A Window to the Science of Tomorrow"*, *J. Synchrotron Radiat.,* vol. 21, p. 837, 2014. doi:10.1107/S1600577514019286

[2] P. F. Tavares, S. C. Leemann, M. Sjöström, and Å. Andersson, *"*The MAX IV Storage Ring Project*"*, *J. Synchrotron Radiat.,* vol. 21, p. 862, 2014. doi:10.1107/S1600577514011503

[3] M. Borland *et al.*, "The Upgrade of the Advanced Photon Source", in *Proc. IPAC'18*, Vancouver, Canada, Apr.-May, 2018, pp. 2872-2877. doi:10.18429/JACoW-IPAC2018-THXGBD1

[4] C. Thomas, G. Rehm, I. Martin, and R. Bartolini, *"*X-Ray Pinhole Camera Resolution and Emittance Measurement*"*, *Phys. Rev. ST Accel. Beams*, vol. 13, p. 022805, 2010. doi:10.1103/PhysRevSTAB.13.022805

[5] H. Sakai e*t al.*, *"*Improvement of Fresnel Zone Plate Beam-Profile Monitor and Application to Ultralow Emittance Beam Profile Measurements*"*, *Phys. Rev. ST Accel. Beams,* vol. 10, p. 042801, 2007. doi:10.1103/PhysRevSTAB.10.042801

[6] D.-C. Zhu, J.-H. Yue, Y.-F. Sui, D.-H. Ji, J.-S. Cao, K.-R. Ye, S.-Q. Tian, J. Chen, and Y.-B. Leng, *"*Performance of Beam Size Monitor Based on Kirkpatrick–Baez Mirror at SSRF*"*, *Nucl. Sci. Tech.*, vol. 29, p. 148, 2018. doi:10.1007/s41365-018-0477-y

[7] T. Naito and T. Mitsuhashi, *"*Very Small Beam-Size Measurement by a Reflective Synchrotron Radiation Interferometer*"*, *Phys. Rev. ST Accel. Beams*, vol. 9, p. 122802, 2006. doi:10.1103/PhysRevSTAB.9.122802

[8] J. Corbett, X. Huang, J. Wu, C. L. Li, T. Mitsuhashi, Y. H. Xu, and W. J. Zhang, "Transverse Beam Profiling and Vertical Emittance Control with a Double-Slit Stellar Interferometer", in *Proc. IBIC'16*, Barcelona, Spain, Sep. 2016, pp. 236-239. doi:10.18429/JACoW-IBIC2016-MOPG70

[9] X. Shi, S. Marathe, M. J. Wojcik, N. G. Kujala, A. T. Macrander, and L. Assoufid, *"*Circular Grating Interferometer for Mapping Transverse Coherence Area of X-Ray Beams*"*, *Appl. Phys. Lett.*, vol. 105, p. 041116, 2014. doi:10.1063/1.4892002

[10] N. Samadi, B. Bassey, M. Martinson, G. Belev, L. Dallin, M. De Jong, and D. Chapman, *"*A Phase-Space Beam Position Monitor for Synchrotron Radiation*"*, *J. Synchrotron Rad.*, vol. 22, p. 946, 2015. doi:10.1107/S1600577515007390

[11] N. Samadi, X. Shi, L. Dallin, and D. Chapman, *"*A Real-Time Phase-Space Beam Emittance Monitoring System*"*, *J. Synchrotron Radiat.,* vol. 26,. p. 1213, 2019. doi:10.1107/S1600577519005423

[12] N. Samadi, X. Shi, L. Dallin, and D. Chapman, *"*Source Size Measurement Options for Low-Emittance Light Sources*"*, *Phys. Rev. Accel. Beams*, vol. 23, p. 024801, 2020. doi:10.1103/PhysRevAccelBeams.23.024801

[13] N. Samadi, X. Shi, C. Ozkan Loch, J. Krempasky, M. Boege, D. Chapman, and M. Stampanoni, *"*A Spatial Beam Property Analyzer Based on Dispersive Crystal Diffraction for Low-Emittance X-Ray Light Sources*"*, *Sci. Rep.*, under review, 2022.

[14] W. H. W. Zachariasen, *Theory of X-Ray Diffraction in Crystals*, New York: John Wiley, 1945.

[15] U. Flechsig, A. Jaggi, S. Spielmann, H. A. Padmore, and A. A. MacDowell, *"*The Optics Beamline at the Swiss Light Source*"*, *Nucl. Instrum. Methods Phys. Res. Sect. A*, vol. 609, p. 281, 2009. doi:10.1016/j.nima.2009.07.092

[16] R. Mokso *et al., "GigaFRoST:* The Gigabit Fast Readout System for Tomography*"*, *J. Synchrotron Radiat.*, vol. 24, p. 1250, 2017. doi:10.1107/S1600577517013522

[17] C. Ozkan Loch, A. Bonnin, J. Vila-Comamala, N. Samadi, A. M. M. Stampfli, and R. Ischebeck, *"*SLS 2.0 – Status of the Diagnostics*"*, presented at IBIC'2022, Krakow, Poland, Sep. 2022, paper MOP01, this conference.

[18] G. Lovric, P. Oberta, I. Mohacsi, M. Stampanoni, and R. Mokso, *"*A Robust Tool for Photon Source Geometry Measurements Using the Fractional Talbot Effect*"*, *Opt. Express*, vol. 22, p. 2745, 2014. doi:10.1364/OE.22.002745

[19] L. Rebuffi and M. Sánchez del Río, *"*ShadowOui: A New Visual Environment for X-Ray Optics and Synchrotron Beamline Simulations*"*, *J. Synchrotron Rad.,* vol. 2, p. 1357, 2016. doi:10.1107/S1600577516013837

[20] L. Rebuffi and M. Sanchez del Rio, *"*OASYS (OrAnge SYnchrotron Suite): An Open-Source Graphical Environment for X-Ray Virtual Experiments*"*, in *Proc. SPIE*, vol. 10388, p. 103880S, 2017. doi:10.1117/12.2274263

[21] M. Sanchez, N. Perez-bocanegra, X. Shi, and V. Honkimäki, *"*Simulation of X-Ray Diffraction Profiles for Bent Anisotropic Crystals*"*, *J. Appl. Crystallogr.*, vol. 48, p. 477, 2015. doi:10.1107/S1600576715002782

Content from this work may be used under the terms of the CC BY 4.0 licence (© 2022). Any distribution of this work must maintain attribution to the author(s), title of the work, publisher, and DOI